Chapter 3

Mussel-inspired adhesive hydrogel patch for wet surfaces with self-healing and pH-dependent drug delivery for potential transdermal applications

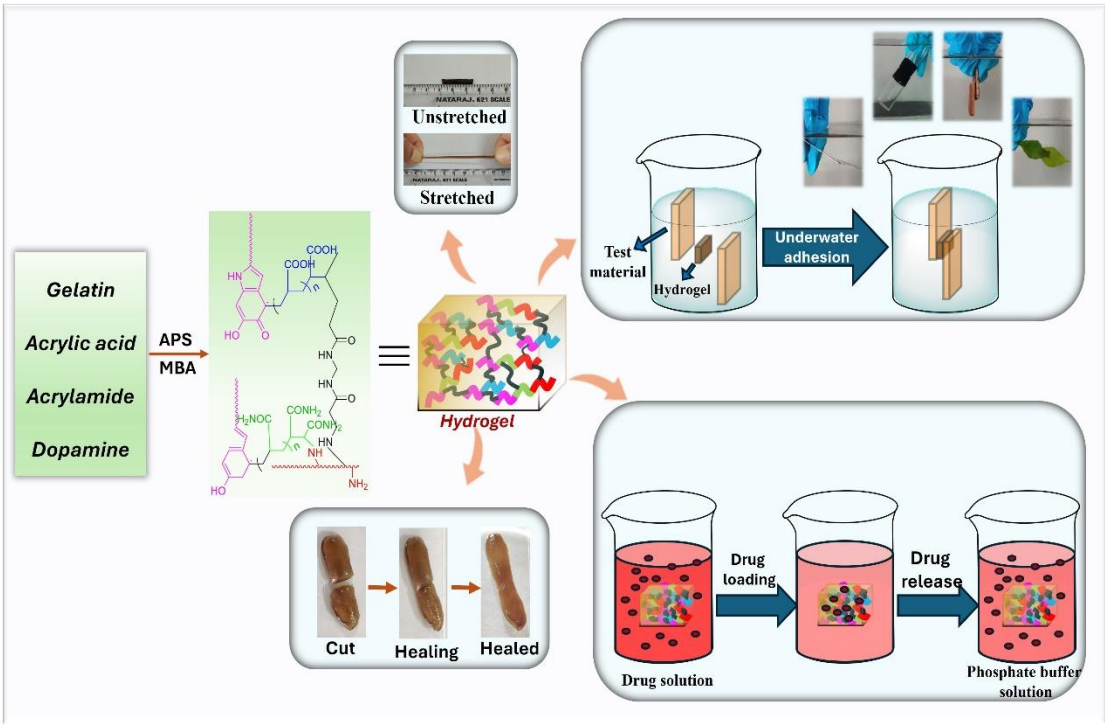

This chapter details the development of adhesive hydrogel, focusing on its dual functionality as an adhesive for wet surfaces and as a pH-responsive drug delivery patch. Additionally, it also emphasizes the repeatable adhesive properties of the hydrogel in both dry and wet environments. The self-healing properties along with its significant mechanical strength have also been highlighted in this chapter.

3.1 Introduction

Adhesives are indispensable in every aspect of our life. From household items, industry, and spacecraft to biomedical areas, the application of adhesives plays a significant role. Since its discovery, innumerable adhesives have been synthesized for various purposes such as in medicine and engineering, and implemented in many areas including sealants [1], soft robotics [2], underwater sensing [3], etc. Specifically, its applications in biomedical fields are highly desirable. However, the relevance of most of the developed adhesives is inadequate for such applications as the exudate that exudes from wounds or other surgical surfaces restrains the adhering substrates from sticking to the skin surfaces. The commonly used adhesives such as cyanoacrylate adhesive solidify immediately on exposure to body fluid, thereby resisting tissue movement [4]. Fibrin-based adhesives possess weak tissue adhesion because of a highly hydrated network [5]. Therefore, adhesives that maintain a well-balanced tissue adhesion under moist or wet conditions are obligatory. In recent years, the application of hydrogels as an adhesive has been widely explored. As discussed in Chapter 1, the soft nature of the hydrogels that mimic natural tissue with their excellent biocompatibility and biodegradability makes them a versatile biomaterial for numerous biomedical applications such as wound healing [6], hemostasis [7], drug delivery [8], tissue reconstruction [9], and wearable electronics [10], and in underwater soft robotics [11-13]. In addition, the applicability of adhesive hydrogels in transdermal drug delivery is magnificent. Painless and non-invasive applications, self-administration of drugs by the patients, and reduced side effects are some of the advantages possessed by adhesive hydrogel as a transdermal patch. Again, the prolonged contact of the adhesive hydrogel to the skin surfaces provides delivery of drugs or other therapeutic agents in a controlled manner thereby promoting wound healing and tissue regeneration [14-19].

Lu and co-workers developed an underwater adhesive hydrogel by rapid UV radiation of methacrylate-functionalized silk fibroin and catechol-conjugated hyaluronic acid and adhered firmly to underwater surfaces [2]. Xue and co-workers introduced a fault-tolerant adhesive hydrogel tape by a novel electro-oxidation process for the oxidation of dopa into dopaquinone in a controlled manner. They demonstrated that hydrogel tape showed great adhesion to various organic and inorganic surfaces through non-covalent interaction [20]. Karthikeyan *et al*. developed a transdermal drug delivery patch by incorporating laponite-confined polydopamine into poly(vinyl alcohol) [21].

Das *et al*. fabricated a polysaccharide-dextrin-based hydrogelator using methacrylic acid as a monomer. The hydrogel shows sustained drug release of amoxicillin at different pH [22]. Although many researchers provide methods to synthesize hydrogel with good adhesion, they fail to meet the ongoing demands from industries and biomedical areas. Alongside potential biomedical applications of adhesive hydrogel in transdermal drug delivery are least explored. Since hydrogel can be endowed with various wound healing properties such as antibacterial [23], antioxidant [24], anti-inflammatory [25], and hemostasis properties, hydrogel can be provided with drugs to promote wound healing.

In the previous chapter (Chapter 2), adhesive hydrogel for wet surfaces has been developed with minimum swelling behavior to ensure maximum adhesion. However, such hydrogel could not act as a drug reservoir because of poor swelling. Therefore, in this chapter, we incorporated acrylamide (AAm) into the previously developed hydrogel system to enhance the swelling property with a well-balanced adhesion to various surfaces under both dry and submerged conditions. In this chapter, a series of adhesive hydrogels have been fabricated *via* a facile one-pot synthesis method. The adhesive performance of the hydrogel has been again studied on various surfaces such as aluminum, glass, tissue surfaces, etc. under both dry and submerged conditions. The hydrogel also demonstrates significant stimuli-free self-healing properties and recyclability that can benefit mainly from the reversible bonding in the catechol group. Thus, the current synthetic procedure opens new possibilities in synthesizing adhesive hydrogel with multifunctional properties for various biomedical applications.

3.2 Experimental section

3.2.1 Materials

Acrylic acid (AA), Acrylamide (AAm), and *N,N′*-methylenebis(acrylamide) (MBA) were purchased from Sigma Aldrich. Dopamine hydrochloride (DA) was purchased from Thermo Fischer Scientific. Gelatin, from porcine skin (type A) was purchased from Himedia. Sodium hydroxide, ammonium peroxodisulfate (APS), and Vitamin B_{12} ($C_{63}H_{88}CoN_{14}O_{14}P$) were purchased from Merck. Deionized water was used during the experiment for preparing various solutions. All the reagents used were of analytical grade and were used as received.

3.2.2 Synthetic procedures

3.2.2.1 Preparation of polydopamine (PDA)

PDA was synthesized following a previously reported procedure [19]. The synthesis was carried out by dissolving a fixed amount of DA powder in an alkaline medium for approximately 15 min or until the color of the transparent solution turned brownish revealing the self-polymerization of dopamine molecules.

3.2.2.2 Preparation of hydrogel

The reaction synthesis follows a two-step procedure. In the first step, a fixed amount of gelatin was dissolved in a round bottom flask at 50°C. AAm was then added to the above solution followed by adding PDA solution to the reaction mixture. The reaction was then initiated by adding free radical initiator APS. In a separate vessel, a certain amount of AAc was mixed with PDA solution which was again initiated by adding APS. Both the solution turns deep red which is the typical color of PDA. Both solutions were then mixed, afterward, MBA was added for the formation of crosslinks within the polymeric chain. The solution was flushed with N_2 atmosphere and was stirred for 1 hr. The brown-colored sticky gel thus formed was washed with deionized water several times. The gel was then allowed to dry at room temperature to evaporate the excess water and the desired adhesive hydrogel was obtained. Detailed compositions of the hydrogels are shown in Table 3.1

Table 3.1: Detailed composition of the hydrogels with varying DA concentration

Hydrogels	*Gelatin (g)*	*AAc (ml)*	*AAm (g)*	*DA (wt%)*	*APS (wt%)*	*MBA (wt%)*
DA2	0.7	0.75	0.45	2	1.5	0.35
DA3	0.7	0.75	0.45	3	1.5	0.35
DA5	0.7	0.75	0.45	5	1.5	0.35
DA6	0.7	0.75	0.45	6	1.5	0.35
DA7	0.7	0.75	0.45	7	1.5	0.35
MB1	0.7	0.75	0.45	5	1.5	0.25
MB2	0.7	0.75	0.45	5	1.5	0.50
MB3	0.7	0.75	0.45	5	1.5	1
MB4	0.7	0.75	0.45	5	1.5	1.5

3.3 Characterization

3.3.1 Structural characterization

Fourier Transformed Infrared Spectroscopy (FTIR), Thermal Stability, Scanning Electron Microscopy, Energy-Dispersive X-Ray Spectroscopy, optical microscopic images, and hemocompatibility of the synthesized hydrogel were carried out using the same instrumentation and specifications as described in section 2.3 in Chapter 2.

3.3.2 Swelling behavior

The swelling capacity of the hydrogels was again measured in a similar way to that in Chapter 2. Since the pH of human skin varies from acidic to basic under different conditions. Hence, in this chapter, to explore the applicability of the synthesized hydrogel as a transdermal patch, the swelling behavior of the hydrogel has been studied at buffered solutions of pH 1.2, 5.8, 7.4, and 8. The equilibrium swelling ratio of the hydrogels was determined by using the formula:

$$\text{Swelling } \% = \frac{W_s - W_d}{W_d} \times 100\%$$

Here W_s and W_d are the weights of the swollen and dried hydrogel samples respectively.

3.3.3 Mechanical strength

The mechanical strengths of the synthesized hydrogels were determined by performing tensile tests using a Universal testing machine (UTM). The as-prepared hydrogel samples were cut into pieces with a dimension of (1mm × 8mm) (thickness × width). The samples were tested at a crosshead speed of 50 mm/min. Alongside, Young's modulus and toughness were calculated. The toughness was calculated by integrating the area under the stress-strain curve.

3.3.4 Adhesive test

Similar to the methods used in Chapter 2 for the adhesion test, in this chapter also, the adhesive strength of the hydrogel on different surfaces was measured using the lap shear adhesion method using UTM. However, a slight modification has been made to the measurement. Here, the curing time for adhesion was kept at 1h, instead of 24 h. For adhesion under dry conditions, a fixed dimension of a hydrogel sample was used to stick two surfaces at room temperature. After 1 hour, the lap-shear adhesion was measured. Similarly, for wet conditions, the two test surfaces were glued together by the hydrogel

under submerged conditions. After a few minutes, the sample was taken from the water and measured after 1 h by a lap-shear method. The reusability of the adhesive hydrogel has been measured on glass surfaces. A standing time of 30 min was given between successive cycles. The adhesive strength is calculated as:

$$\text{Strength} = \frac{Maximum\ load}{Bonded\ area}$$

3.3.5 Self-healing experiment

The self-healing ability of the hydrogel was characterized by comparing the tensile strength of the hydrogel before and after healing using UTM. For measuring, hydrogel samples of dimensions (5 mm × 3.5 mm) (width × thickness) were first stretched until broken, and the tensile strength was determined. The surface of the broken hydrogel sample was immediately brought into contact and was stored in an air-tight vessel for 24 hr. The tensile strength of the completely healed hydrogel was then again measured. The self-healing was also determined by the optical microscopic image. A thin film of hydrogel was cut and then immediately brought into contact. Optical microscopic images of the cut and healed hydrogel film were recorded.

3.3.6 In-vitro degradation studies

The degradation of the synthesized hydrogel has been determined by immersing a dried hydrogel sample in a PBS of pH 7.4. It was then incubated at 37 °C for varying periods. The samples were taken out and washed with deionized water to remove the degraded products. The mass of the dried samples before and after degradation were measured. The residual mass percentage has been calculated using the formula

$$\text{Residual mass (\%)} = \frac{W_0 - W_t}{W_0} \times 100\%$$

Here W_o and W_t are the masses of the hydrogel before and after degradation.

3.3.7 *In vitro* cytotoxicity evaluation

To evaluate cell viability, mouse fibroblasts (L929) were seeded in a 96-well plate at 1×10^4 cells per well. Each well received 200 µl of Dulbecco's Modified Eagles Medium (DMEM) with 10% Fetal bovine serum (FBS) and 2% antibiotic antimycotic was purchased from Gibco, ThermoFisher Scientific, and the cells were left to grow overnight in a humidified CO_2 incubator at 37°C. The following day after seeding, the cells were exposed to 200 µl of various dilutions of sample extracts (1X, 2X, 5X, and

10X of the original extract diluted with FBS-supplemented DMEM). The extract was prepared by immersing a 1 cm × 1 cm sample in 4 ml of media, agitating at 120 rpm at 37 °C for 72 h, and filtering through a 0.2 µm sterile membrane. In control, cells were cultured in standard media containing 10% FBS and 2% antibiotic-antimycotic. After 72 h, 20 µl of MTT solution was added to each well and incubated for 3 h. Following this incubation, 100 µl of DMSO was added to each well, and absorbance was measured at 570 nm using a Clariostar Plate Reader. Cell viability percentage was then calculated using the following equation.

$$\text{Cell viability (\%)} = \frac{OD_{570nm}treated}{OD_{570nm}control} \times 100$$

The live-dead assay was conducted by staining cells with calcein AM (which stains live cells) and ethidium bromide (which stains dead cells) in incomplete DMEM media for 40 minutes at 37 °C in a humidified incubator following three days of fibroblast incubation with sample extract. Samples were stained and subsequently rinsed with PBS before imaging using a Leica fluorescence microscope (Ex = 501 nm, Em = 521 nm, and Ex = 301 nm, Em = 603 nm for calcein AM and ethidium bromide, respectively). The results were expressed as the mean ± SD, and the viability measurement was performed in triplicate.

3.3.8 Drug loading and release study

Vitamin B_{12} has been used as a model drug to study the drug loading and releasing effect. The drug loading in the hydrogel was carried out by the soaking or equilibrium method. A fixed weight of the hydrogel sample was first swelled in a buffer solution of pH 7.4 to determine the exact amount of solution required to achieve an equilibrium swelling. A calculated amount of drug was dissolved in the above-calculated buffer solution and the hydrogel sample was immersed to absorb the drug. The drug-loaded hydrogel was then dried at 40 °C.

The drug release study was performed at PBS at pH 5.8 and 7.4. The drug-loaded hydrogel sample was immersed in a 5ml PBS of the required pH at room temperature. 1 ml of aliquot was taken out at an interval of 30 min and was determined spectrophotometrically using a UV-visible spectrophotometer. 1 ml of PBS of the same pH was added to the drug solution to maintain a constant volume. The drug release by

the hydrogel was then determined by calculating the cumulative release percentage from a standard curve that was calibrated beforehand.

3.4 Results and Discussion

3.4.1 Synthesis of hydrogel

The adhesive hydrogel was synthesized by following a facile synthetic method. In the first step, DA was oxidized to form PDA by dissolved oxygen. The oxidation of DA was triggered by a basic medium (pH 10). It occurs through a multistep process where DA first oxidizes to form dopaminequinone (DQ) followed by intermolecular cyclization *via* 1,4-Michael addition and finally polymerizes to give PDA. The polymerization of PDA can be seen from the change in color of the transparent DA solution to an opaque brown color, which is the typical color of PDA [26-30]. In the second step, PDA was grafted to a solution of Gel/AAm and AAc respectively using APS as an initiator. Both the solutions were mixed, and MBA was added to get the crosslinked product. Since overoxidation of PDA often inhibits the polymerization process. Therefore, the addition of AAc is the key factor during the synthesis process as it prevents overoxidation of PDA by maintaining an acidic environment and providing a balance between the adhesive and cohesive properties. In addition, AAc also improves the mechanical strength and pH stimuli responsiveness of the hydrogel. The PDA also forms a non-covalent interaction with the polymeric network of gel/AAm/AAc through π-π stacking and H-bonding. The plausible mechanism of the formation of hydrogel is shown in Scheme 1. This hybrid crosslinking of PDA to the gel/AAm/AAc network by both covalent and non-covalent interaction leads to sustained deformation, reversible adhesion, and self-healing ability. A schematic diagram showing crosslinking of polymers to form hydrogel is shown in Figure 3.1.

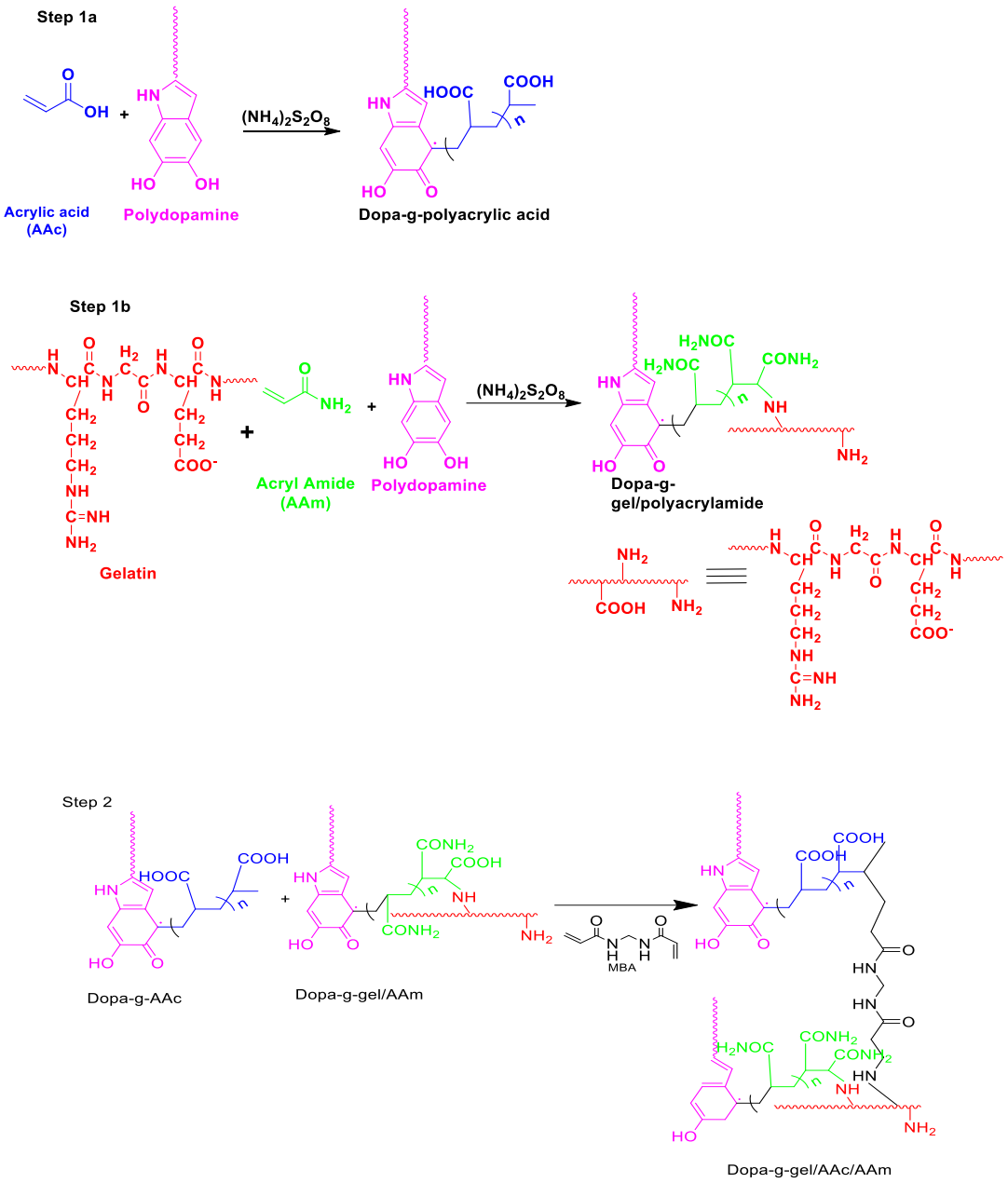

Scheme 3.1: Plausible mechanism of hydrogel formation

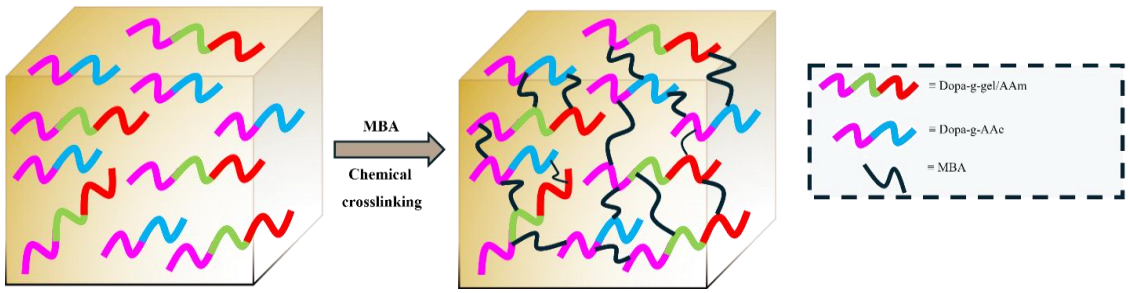

Figure 3.1 Schematic diagram showing crosslinking of polymers to form hydrogel

3.4.2 FTIR analysis

The possible interaction between the monomer and the hydrogel formation can be determined from FTIR spectroscopy. The FTIR spectra of the hydrogel with different compositions of DA are shown in Figure 3.2(a) and the corresponding spectra for the monomer molecules are shown in Figure 3.2(b). The characteristic peaks at 3446 cm^{-1} and 2927 cm^{-1} for gelatin molecules were attributed to the presence of -NH_2 and CH_2 group respectively. Again, the peak at 1650 cm^{-1} is due to N-H bending [31,32]. For acrylic acid, the broad band at 3458 cm^{-1} is due to O-H stretching and the characteristic band around 1700 cm^{-1} resulted from the vibration of the carbonyl group of the carboxylic acid [33]. For acrylamide, the strong absorption peak around 3300 cm^{-1} and at 1679 cm^{-1} are characteristics of –NH_2 and amide groups respectively. The peak around 900 cm^{-1} confirmed the presence of alkene and C-H bending [34]. The spectrum shows significant differences between the hydrogel's monomers and the hydrogel. In the spectra of AAm and AAc, the peak around 900 cm^{-1} which is due to the vibration of H in C=C-H is very clear, but it gets diminished in the spectra of the synthesized hydrogel, meanwhile, the peak at 1164 cm^{-1} which is prominent in the hydrogel indicated the C-C bond suggesting the successful polymerization of the monomer. Again, the peak at 3447 cm^{-1} due to N-H stretching becomes sharp in the hydrogel spectra due to the formation of the network structure. Similarly, the hydrogen bond stretching vibration of methylene in the spectra of synthesized hydrogel is stronger indicating the reduction of the C=C bond which becomes saturated after the polymerization process. The NH stretching in the hydrogel was established by the peak at 1642 cm^{-1}. The peak at 1456 cm^{-1} resifted from the deformation stretching vibration of the methylene group. Thus, the occurrence of new peaks and re-shifting of old peaks demonstrate the successful formation of hydrogel.

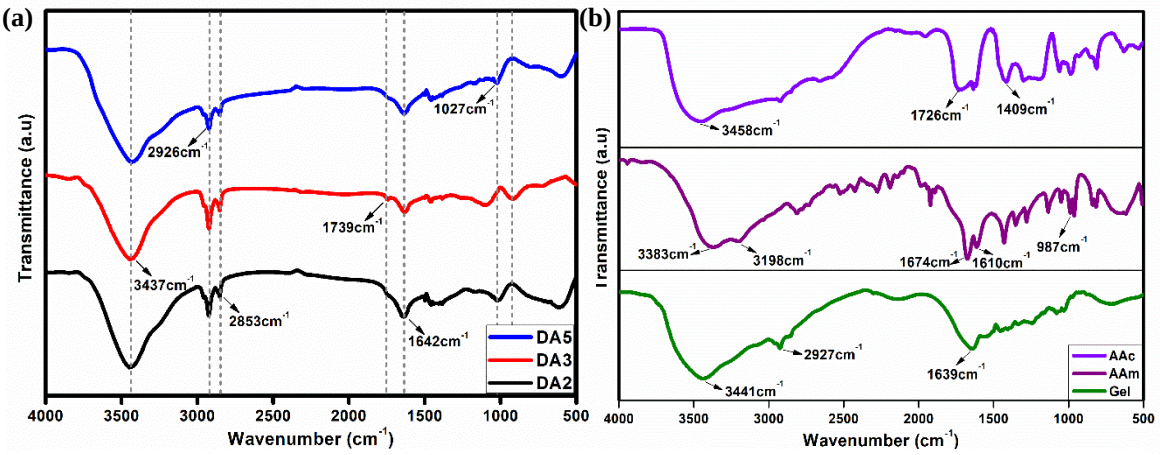

Figure 3.2 FTIR Spectra of (a) hydrogel at different DA content and (b) monomers

3.4.3 SEM analysis

The microstructure of the synthesized hydrogel has been characterized using scanning electron microscopy. The SEM image of the air-dried sample shows the smooth surface of the hydrogel. (Figure 3.3(a)). However, a crack in the hydrogel depicts its porous structure as shown in Figure 3(b). This is due to the surface tension effects which arise on water evaporation, leading to cracks or surface artefacts. The distribution of the elements C, O, and N has been well established using elemental mapping and is presented in Figure 3.3 (c).

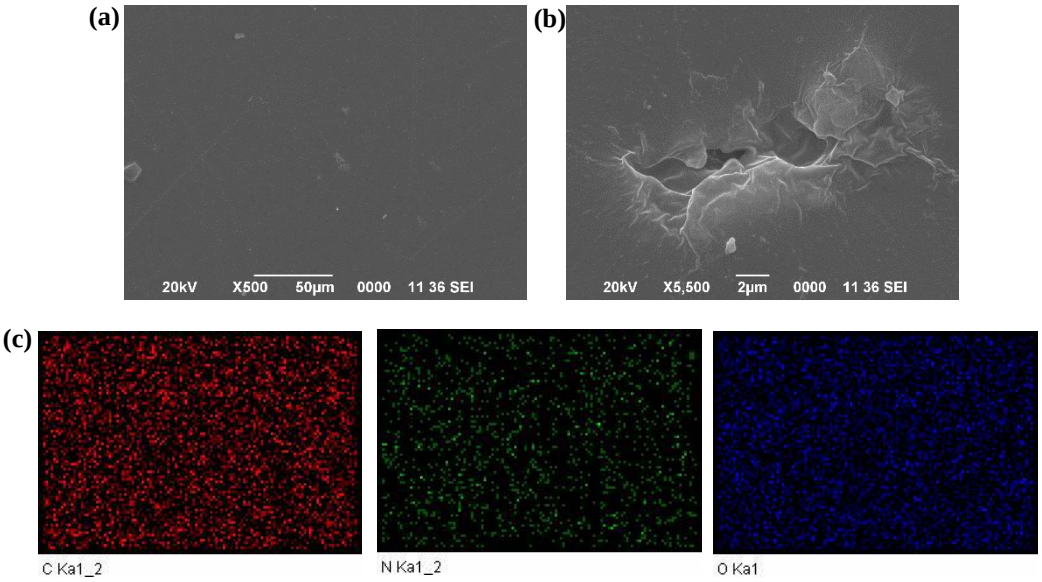

Figure 3.3 (a), (b) SEM images of the hydrogel; (c) elemental mapping of carbon, oxygen, and nitrogen of the hydrogel

3.4.4 Thermal degradation study and XRD analysis

The thermogravimetric analysis (TGA) results as depicted in Figure 3.4(a), reveal that the hydrogel is relatively stable and can be applied under a wide range of temperatures. The initial weight loss of 4% between 100 °C‑150 °C is due to the loss of moisture content within the gel matrix followed by a gradual decrease in weight up to around 360 °C. This decrease in weight percentage of 30 % occurs mostly due to the decomposition of functional groups. Further, a steep decrease in weight at higher temperatures results from the degradation of C-C bonds in the polymeric chain. Again, no significant change has been observed in hydrogels with different ratios of DA.

Again, the XRD spectra of the hydrogel showed a broad band at $2\theta=20°$, which is the characteristic peak of gelatin (Figure 3.4(b)). This broadband depicts the amorphous nature of the hydrogel [35,36].

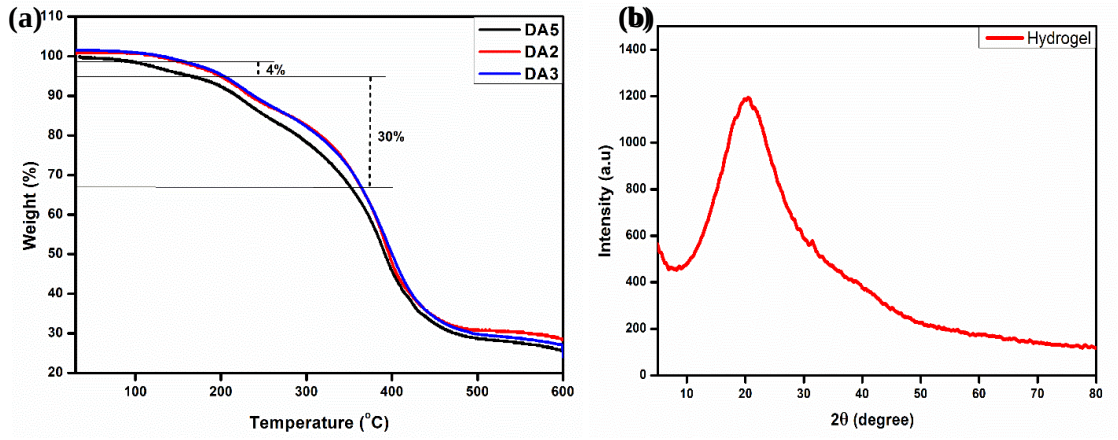

Figure 3.4 (a) TGA spectra at different DA content and (b) XRD spectra of hydrogel

3.4.5 Swelling behavior

The swelling behavior of the hydrogel plays a key role in determining the stability of the adhesive hydrogel, since most hydrogels when fully swollen lose their adhesive behavior. Again, a hydrogel with poor swelling properties is inappropriate for some applications such as drug delivery and wound healing. Therefore, it is necessary to synthesize hydrogel with optimum swelling behavior to satisfy its application for different purposes. In general, the swelling of hydrogel depends on its cross-linking ability. Here, we investigated the swelling behavior of synthesized hydrogel by varying the crosslinker content from 0.25 wt% to 1.5 wt% and swelled under a phosphate buffer solution of pH 5.8, 7, and 7.4. From Figure 3.5(a), it was found that on decreasing the crosslinker content, swelling of the hydrogel gradually increases. This is because of the decreasing crosslinking density which allows the water molecules to penetrate within the three-dimensional network. In addition, the swelling behavior of the hydrogel at different pH conditions of 1.2, 5.8, 7, 7.4, and 8 have also been studied. It is evident from Figure 3.5(b) that the equilibrium swelling ratio of the hydrogel increases with an increase in pH. At acidic pH i.e. at pH 1.2, the hydrogel shows an equilibrium swelling ratio of 219% which is the lowest compared to its swelling at higher pH. This can be due to the non-ionized form of the hydrophilic groups such as -COOH, -OH, and -NH at lower pH which restricts the formation of H-bonding with water molecules thereby decreasing the swelling ratio. However, when the pH is increased to 8, the equilibrium swelling ratio gradually increases. This is because at higher pH, the hydrophilic group becomes deprotonated, and the negatively charged carboxylic ion causes repulsion within the hydrogel network thereby increasing the swelling ratio.

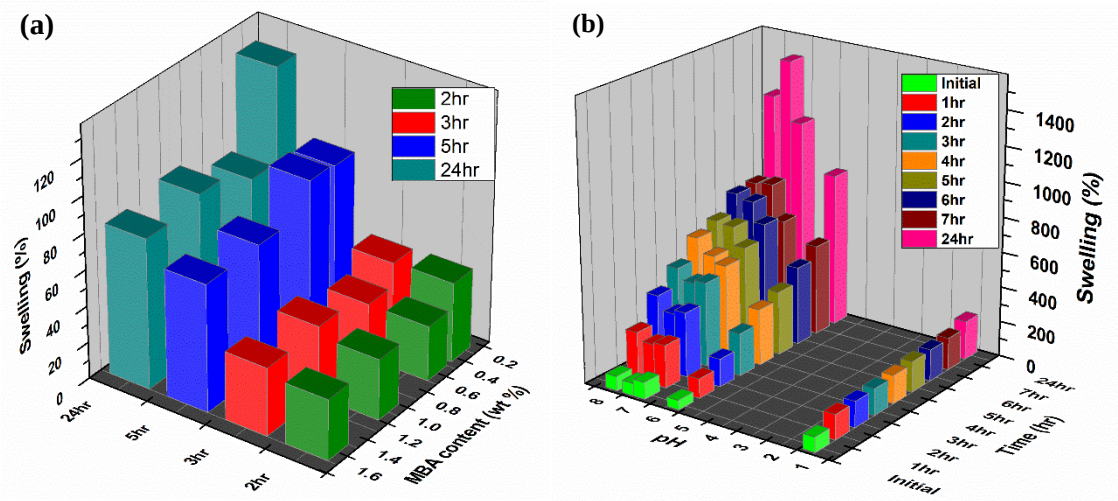

Figure 3.5 Swelling behavior of the hydrogel with (a) varying crosslinker content and (b) at different pH

3.4.6 Tensile strength

The hydrogel appears to be stretchable and highly resilient. It is challenging to develop an adhesive hydrogel with relevant mechanical properties. Here, the mechanical properties of synthesized hydrogel have been studied *via* tensile testing. As seen in Figure 3.6, hydrogels with different ratios of dopamine and MBA show different mechanical strengths depicting tunable mechanical properties of the hydrogel. In Figure 3.6(a), DA5 denotes hydrogel with DA content of 5wt%, and DA6 and DA7 denote hydrogel with 6wt% and 7wt% DA content respectively. It was found that DA5 has shown superior hydrogel strength with tensile stress of 5.38 MPa. On further increasing the concentration of DA to 6wt% and 7wt%, the tensile stress decreases rapidly to 3.29 MPa and 0.968 MPa respectively. This might be due to the interference of the hydroxyl group in DA moiety that was overoxidized by APS, thus inhibiting the polymerization process resulting in a decreased mechanical strength of the hydrogel. On the other hand, increasing the content of DA from 5wt% to 7wt%, tensile strain increases which again results from the poor polymerization causing the hydrogel to be softer and more flexible with the addition of DA content. In addition, the toughness of DA5 hydrogel was found to be 7.285 MJm^{-3} with Young's modulus of 40.67 KPa which is comparatively higher than both DA6 and DA7 (Figure 3.6(b) and (c)). The high toughness of DA5 hydrogel allows it to maintain its functionality under pressure. Similarly, the effect of crosslinker MBA on the mechanical strength of hydrogel can be seen in Figure 3.6(d). Increasing the MBA content from 0.25wt% to 1.5wt%, there is a gradual decline in tensile stress. The hydrogel with MBA content of 0.25wt% showed a tensile strength of 4.04 MPa which

decreased to 1.56 MPa with an MBA content of 1.5 wt%. This decrease in tensile stress results from the rapid crosslinking within the polymeric network, making the hydrogel less resilient to external stress thereby reducing the tensile strain. The Young's modulus and toughness of the hydrogel with varying MBA content are shown in Figure 3.6 (e) and (f). Moreover, the high mechanical strength of the hydrogel can be seen in Figure 3.7 (a) where DA5 hydrogel with a dimension of 0.84 mm × 8.94 mm can lift a weight of 2.4 g.

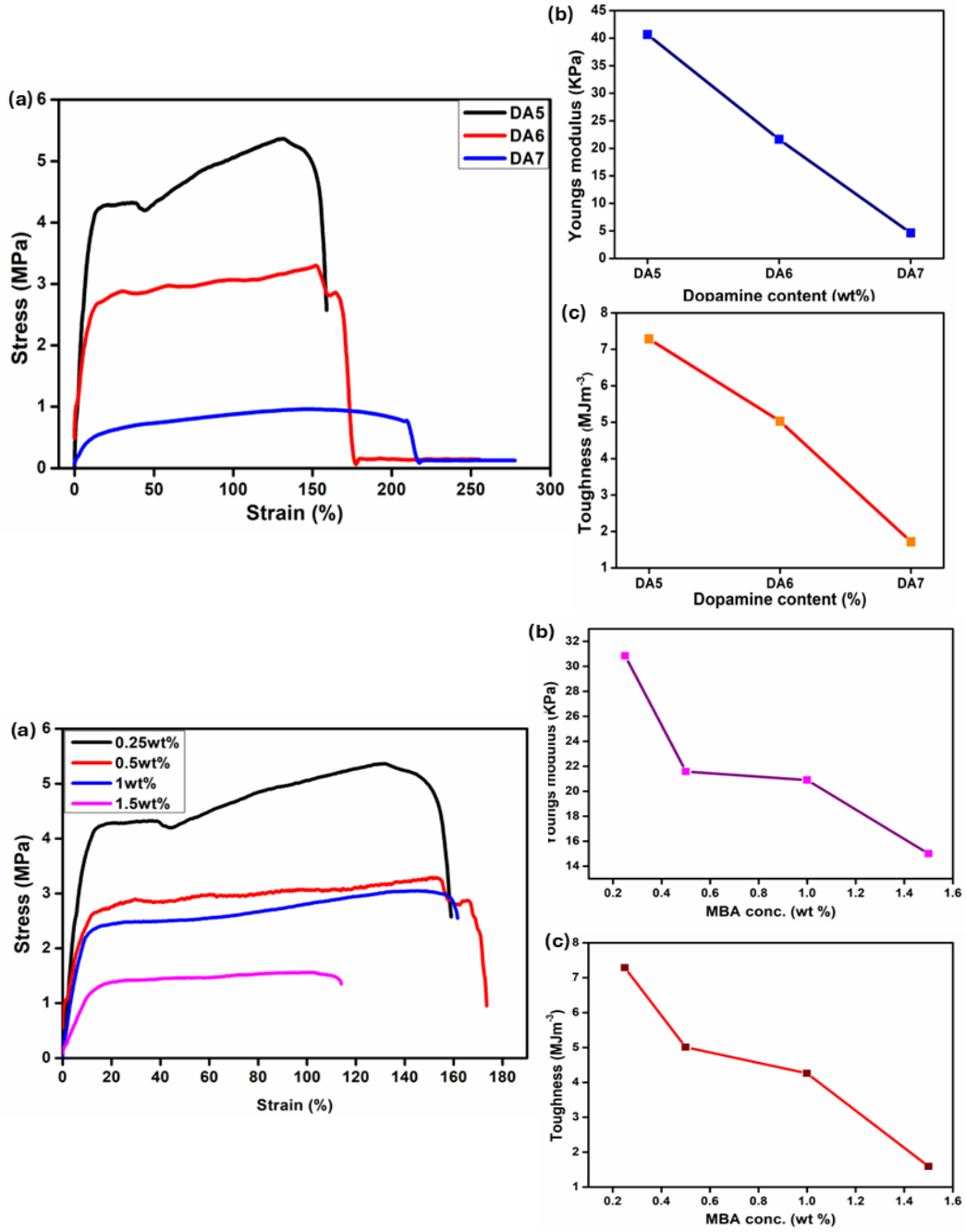

Figure 3.6 Tensile strength of the hydrogel at different content of (a) DA, (d) MBA; (b)Young's modulus and (c) toughness of hydrogel with varying content of DA; (e) Young's modulus and (f) toughness of hydrogel with varying content of MBA

Again, for certain applications, hydrogels are required to bear repetitive stress. Therefore, the cyclic stretching of the synthesized hydrogel was carried out for 3 consecutive cycles and their tensile strength was measured. It was found that on 2nd cycle, the tensile strength of the hydrogel was reduced by only 13%. This is due to the rapid deformation of the noncovalent bond like H-bond within the hydrogel matrix. Again, on the 3rd cycle, the tensile strength is higher than in the 2nd cycle because the deformed covalent bond got enough time to recover and hence the tensile strength increases. From Figure 3.7 (c), it was found that for up to 3 cycles, the hydrogel doesn't show high variation in its tensile strength. This indicates the reversible stretchability of the hydrogel. In addition, it also implies its high flexibility which was further evaluated. Figure 3.7 (b) shows a piece of hydrogel after being twisted, returned to its original shape immediately after removing the stress. Moreover, hydrogels with transparent properties are advantageous for various applications for easy monitoring of the internal structures during their application. Therefore, the optical transparency was checked by placing a thin film of hydrogel with a thickness of 1mm over the word "HYDROGEL" and it was found that the gel was sufficiently transparent as the word is distinctly visible. (Figure 3.7(b))

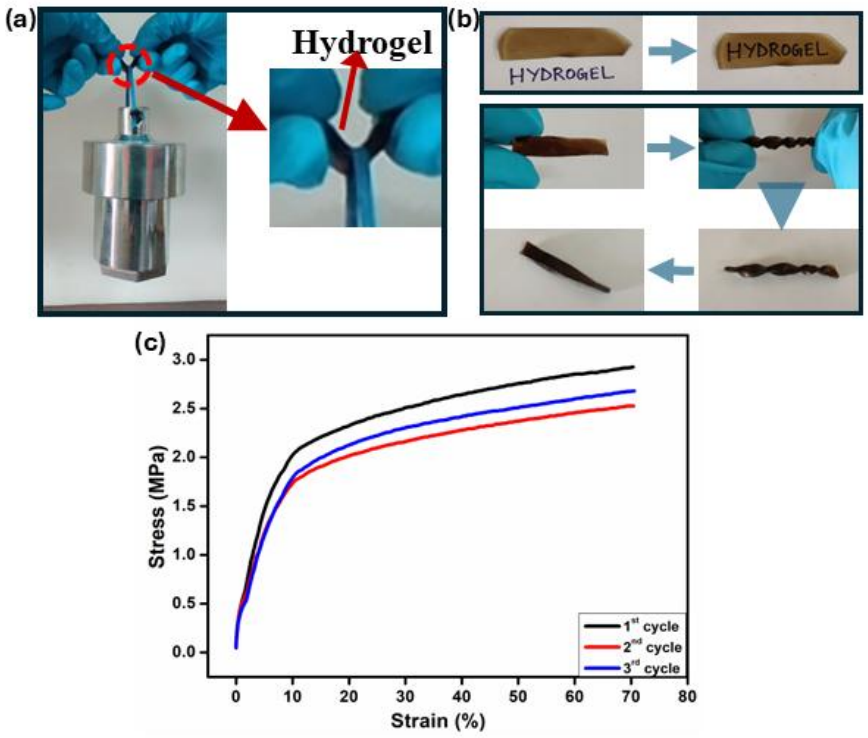

Figure 3.7 Digital image showing (a) a piece of hydrogel lifting a weight of 2.4 kg, (b) showing transparency and flexibility of hydrogel (c) repeatable stretching of the hydrogel

3.4.7 Self-healing

Due to the prolonged use of hydrogel on various surfaces, it is of utmost importance for the hydrogel to possess the self-healing ability to withstand cracks or any other damage during its application. Therefore, the self-healing behavior of the hydrogel was quantitatively investigated by the tensile testing method, and macroscopic and microscopic analyses were also carried out. From Figure 3.8(a) we have seen that the tensile strength of the original hydrogel was found to be 0.1 MPa, and that of the self-healed hydrogel is 0.2 MPa both showing tensile strain around 250%. The increase in tensile strength in the self-healed hydrogel may be attributed to the moisture loss during the self-healing process making the hydrogel tougher. Again, from Figure 3.8(b), the optical image shows that when the two pieces were cut and brought together immediately showed self-healing behavior as the joint between the two cut pieces disappeared while keeping the hydrogel under closed condition for 12 hrs. In addition, the microscopic

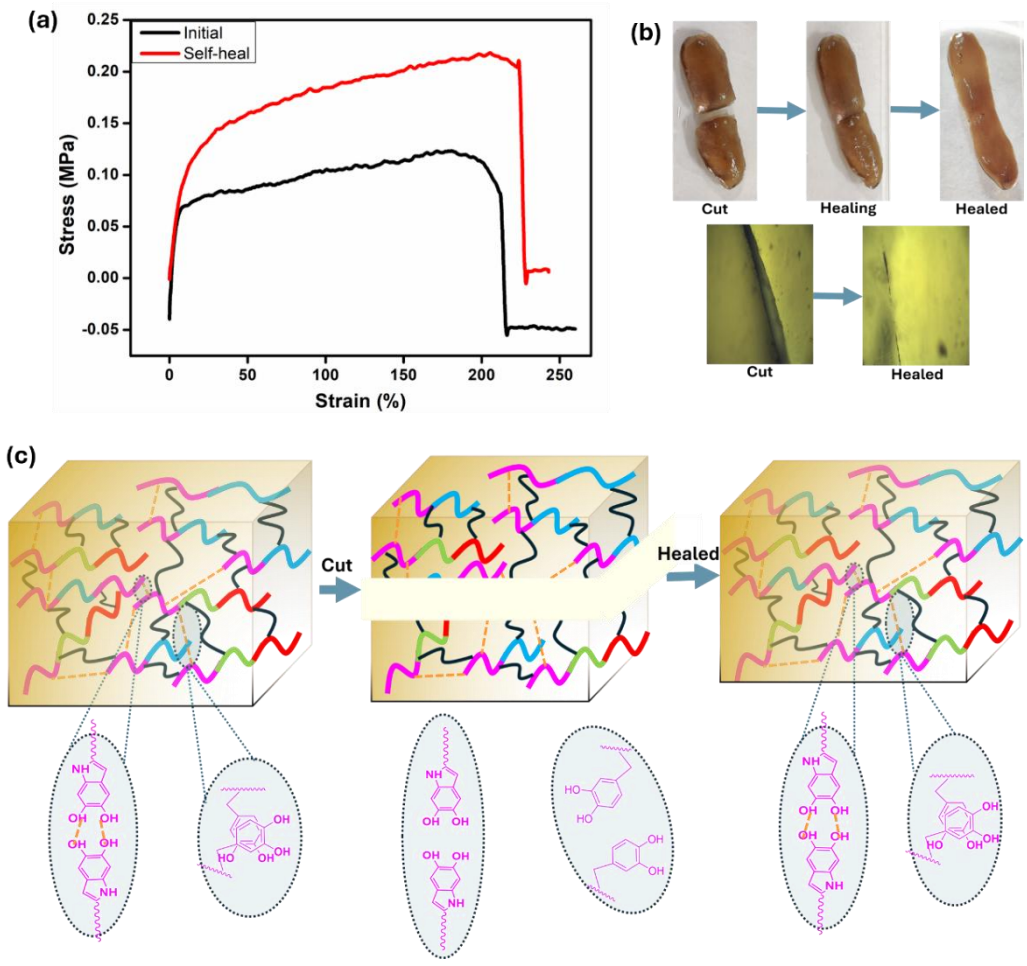

Figure 3.8 (a) Tensile strength of the hydrogel before and after self-healing; (b) Digital and microscopic image of the hydrogel during self-healing; (c) Schematic diagram of the hydrogel showing the self-healing mechanism

image taken by a polarizing microscope also reveals that the hydrogel started to self-heal within 30 minutes when a thin film was considered (Figure 3.8(b)) The presence of dopamine molecules imparts stimuli-free self-healing behavior to the hydrogel matrix. This self-healing behavior can be attributed to the dynamic covalent and non-covalent interactions within the hydrogel. Since the two cut surfaces contain active catechol groups, when the two cut surfaces are immediately brought together, the Schiff base reaction and hydrogen bonding and π-π interaction start forming between the two cut surfaces. A schematic diagram of the hydrogel with possible interaction during the self-healing process is shown in Figure 3.8(c).

3.4.8 Adhesion

The adhesive property of a hydrogel is an important aspect of its application in various biomedical areas such as in tissue and other synthetic substances for biomedical implants, wearable devices, and soft robotics. In this chapter again, we studied the adhesive behavior of the synthesized hydrogel to various substrates under both dry and wet conditions by the lap-shear adhesion method. The hydrogel with the highest mechanical strength as found from the tensile test has been considered for adhesion study. Figure 3.9(b) shows the adhesion of the hydrogel towards different substrates under both dry and wet conditions. Moreover, the adhesion of the hydrogel towards human skin and the mechanism behind the adhesion are shown in Figure 3.9 (c) and (d). The adhesive strengths for different substrates such as aluminum and glass sheets were 40 kPa and 120 kPa respectively. The higher adhesive strength of hydrogel towards glass is due to the formation of stronger covalent interaction compared to its interaction with aluminum sheets. Similarly, under wet conditions, i.e. when performed the adhesive experiment under submerged conditions, the adhesive strength for aluminum and glass was found to be 20 kPa and 30 kPa respectively. Furthermore, the adhesive strength of the hydrogel on goat tissue under dry and wet conditions has also been evaluated. The adhesive strength of the hydrogel on goat tissue under dry conditions was found to be 45 kPa and in wet conditions, the strength was found to be 14.5 kPa. The adhesive strengths are shown in Figure 3.9(e). The adhesive behavior of the hydrogel on tissue surfaces is mainly due to the formation of a dynamic imine bond between the free catechol group in the hydrogel and the amide or amine group in the tissue surfaces. Again, under wet conditions, the aromatic group of dopamine molecules present in the hydrogel surfaces provides a hydrophobic environment on the surfaces thereby restricting the formation of

a hydration layer on the interfacial surface thus promoting wet adhesion [37,38]. However, prolonged immersion of the test subject under water reduces the adhesive strength that results from the hydrogel's swelling under wet conditions.

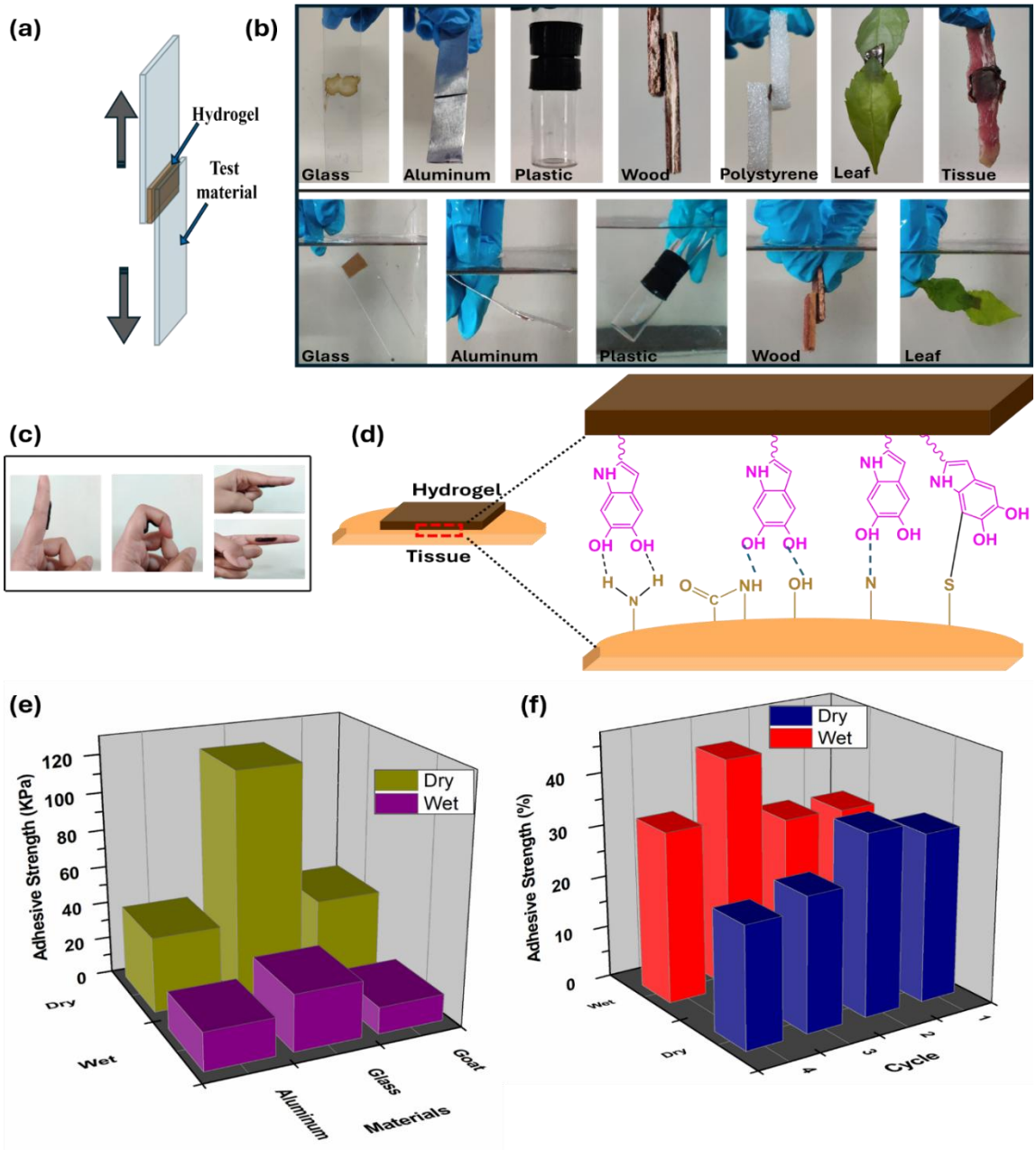

Figure 3.9 (a)Graphical image showing lap-shear adhesion test; (b) optical images showing adhesion of the hydrogel to different substrates; (c) Digital images showing adhesion to human skin; (d) Schematic diagram showing possible interactions of hydrogel with biological tissue surface; (e) adhesive strength of the hydrogel under both dry and wet conditions; (f) Repeatable adhesion of the hydrogel up to 4 cycles

Many adhesives showed permanent adhesion and when displaced lose their adhesive property hindering their long-term applicability on diverse surfaces. Therefore, the reversible adhesive property in a hydrogel is of paramount importance. A cyclic test has been performed to determine the reversibility of the synthesized hydrogel and it was found to have reversible adhesiveness under both dry and wet conditions. The reversibility was checked on a glass substrate for the dry adhesion cycle. A thin piece of hydrogel has been used to adhere the two surfaces. The lap-shear adhesion was performed after 30 min and after the test, two surfaces were joined together immediately using the same adhesive hydrogel. The experiment has been carried out for up to 4 cycles with an interval of 15 min. As shown in Figure 3.9(f), in the second cycle there is a slight increase in the adhesive strength due to the formation of new H-bonding during destruction-construction of the hydrogel network [39]. However, on repeating further, there is a decline in the adhesive strength which may be due to the rupture of the original bond within the hydrogel network. Similarly, for the wet adhesive cycle, the two glass substrates were joined together by a thin piece of hydrogel under submerged conditions, and the lap-shear adhesion test was carried out after 30 min. The adhesive test was performed up to 4 cycles. This reversible adhesion of the hydrogel with different substrates is attributed mainly to the presence of reversible non-covalent interactions such as H-bonding, imine bond, π-π interaction, van der-Waals interaction, etc., within the surface of the hydrogel and the test material.

3.4.9 *In vitro*-hemocompatibility and degradation

The *in vitro* biocompatibility of synthesized hydrogel has been determined by performing a hemolysis test. For the ongoing demand for adhesive hydrogel for various biomedical applications, it is necessary to determine its hemocompatibility. The quantitative analysis as shown in Figure 3.10 reveals that the hydrogel with a weight of 0.5 mg shows very little hemolysis of 3.73% and hydrogel with a weight of 1 mg shows hemolysis of 5.28 %. This value is within the permissible limit of 5%. Thus, this established the biocompatible nature of the hydrogel and hence is suitable for its application as an adhesive in numerous areas.

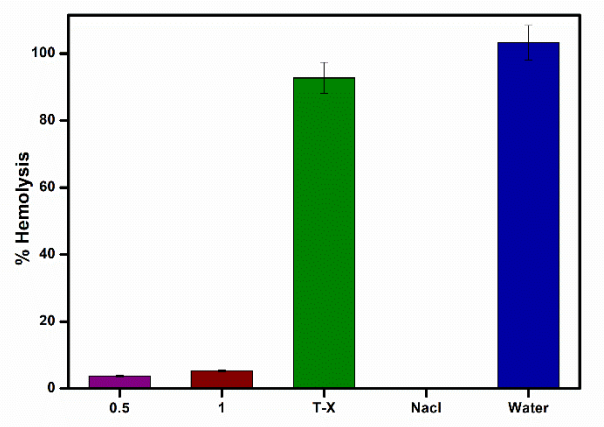

Figure 3.10 Hemocompatibility of the hydrogel

The in-vitro degradation of the adhesive hydrogel was estimated from the change in weight of the hydrogel after incubation in PBS at pH 7.4. It was found that the hydrogel undergoes weight loss of 60 % within 11 days. This implies good biodegradation of the hydrogel that is beneficial for further *in vivo* applications. Degradation in basic buffer solution generally proceeds through the structural degradation of the crosslinker MBA. The methylene group in MBA has a partial positive charge and hence can be easily attacked by nucleophilic water thereby breaking the molecule [40,41]. This scission can be confirmed by comparing the FTIR spectra of the undegraded and degraded hydrogel as shown in Figure 3.11. The sharp peak at 3446 cm^{-1} is due to the N-H bond in the undegraded hydrogel becoming broader in the degraded hydrogel which might be attributed to the formation of hydrogen bonds and the introduction of new hydroxyl groups. Similarly, the peak at 1639 cm^{-1} becomes broader in the degraded hydrogel due to the conversion of -$CONH_2$ to -COOH groups. In addition, the small peak around 1100 cm^{-1} due to C-N-C of MBA undergoes major changes and a broad peak appears in the degraded hydrogel. This indicates the scission of C-N-C bond and the formation of a new hydroxyl group. Thus, these changes and shifts in peak intensities indicate the degradation of the hydrogel in a buffer solution of pH 7.4.

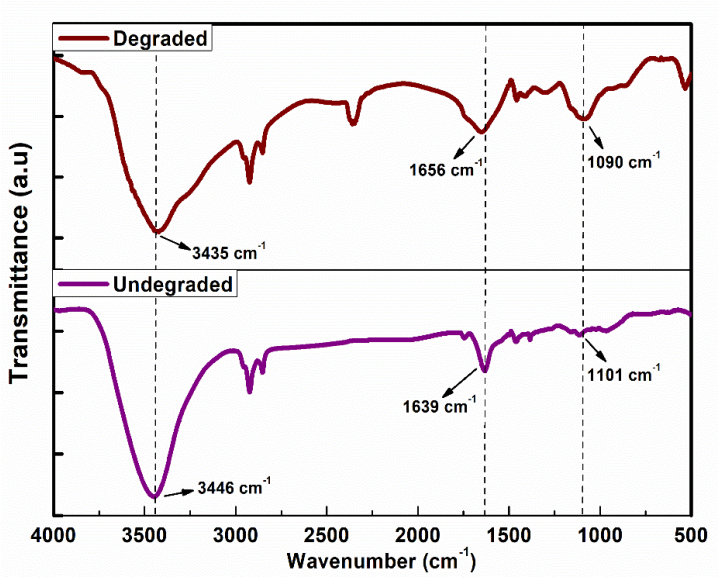

Figure 3.11 FTIR spectra of the undegraded and degraded hydrogel

3.4.10 Determination of cell bio-compatibility

3.4.10.1 Determination of Cell Proliferation Activity

The biocompatibility of the synthesized hydrogel is further evaluated by conducting a cytotoxicity test using four different concentrations of the hydrogel extract. Figure 3.12 demonstrates that the extract's concentration significantly influences the test results. The cell viability assessment, as illustrated in Figure 3.12(a), indicates a cell viability of 45.94% in the presence of a highly concentrated (1X) gel extract. This observation may be attributed to the release of the unreacted acrylamide group from MBA and poly(acrylamide) during the extraction process. However, 5X and 10X dilutions of the hydrogel extract maintained cell viability above 85%.

3.4.10.2 Live/dead cell viability assay

Additionally, a live/dead cell viability assay of the hydrogel extracts was performed, and the images are presented in Figure 3.12(b). These images reveal that increasing the dilution of the extract corresponds to an increase in the number of viable cells. Consequently, these findings suggest that at low concentrations, the hydrogel does not induce significant cell mortality and can therefore be considered relatively cytocompatible.

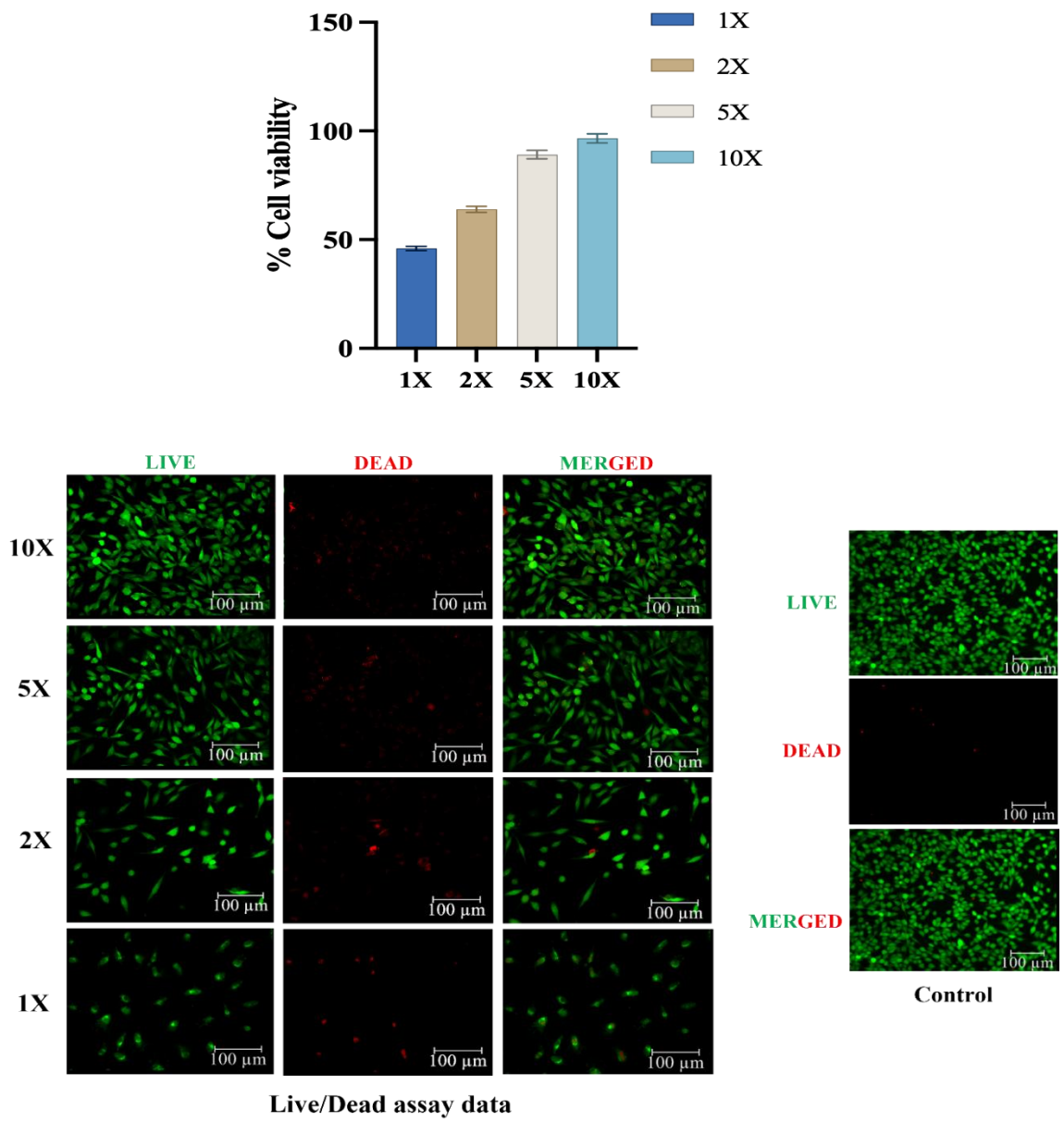

Figure 3.12 (a) cell viability assay of the hydrogel extract at different dilutions, (b) Representative live/dead staining images of L929 fibroblast cells after incubation with the hydrogel extract for 3 days

3.4.11 Drug adsorption and release study

The adhesiveness of hydrogel to human skin emphasizes its applicability as a therapeutical patch for wound healing or as a transdermal drug delivery patch. In addition, the swelling behavior of the hydrogel depicts its pH sensitivity. Therefore, we have studied the drug release performance of the hydrogel at two different pH. The drug loading of the hydrogel can be characterized by comparing the FTIR spectra of hydrogel with and without Vitamin B_{12}. As seen in Figure 3.13, the FTIR spectra of the Vitamin

B_{12} loaded and unloaded hydrogel show no significant change in the peaks. However, the intensity of the peak at 3441 cm^{-1} and 2927 cm^{-1} increases. This increase in peak intensity is due to the N-H stretch of amide linkage and the C-H stretch of methylene group in Vitamin B_{12}.

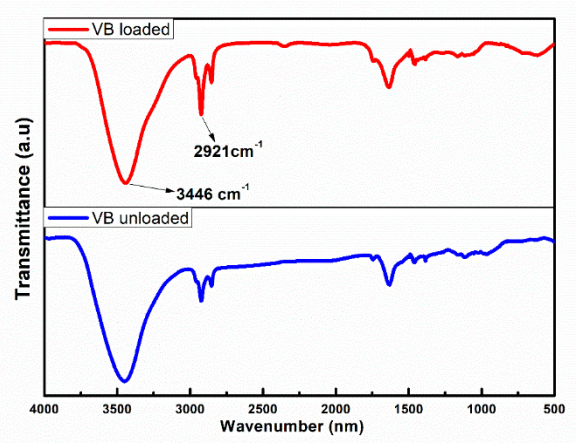

Figure 3.13 FTIR spectra of the Vitamin B_{12} loaded and unloaded hydrogel

For its applicability in transdermal drug delivery, *in vitro* drug release was performed in a buffer solution of pH 5.8 and 7.4 which is the pH of healthy and infected skin respectively [42,43]. When the hydrogel is swollen at the desired pH solution, diffusion occurs in the first step. In this step, the drug molecules on the surface of the hydrogel diffuse to the solution. In the second step, water molecules permeated into the 3D hydrogel network causing the drug molecules to get released in the solution. Figure 3.14 shows the drug release efficiency of the hydrogel at different pH. The cumulative drug release percentage of vitamin B_{12} is found to be pH-dependent. It was found that within 4 hours the drug-loaded hydrogel at pH 5.8 showed a drug release of 36.18% and at pH 7.4, it showed a drug release of 59.70%. This higher drug-release behavior at pH 7.4 is due to the higher swelling effect caused by appreciable ionization at higher pH, leading to faster drug molecule release than at pH 5.8. On further swelling within 8 h, the drug release at pH 5.8 increases to 60%, and at pH 7.4, it shows a release of 96%. However excess swelling at pH 7.4 results in deterioration of the hydrogel properties. This pH-dependent drug release is favorable for wound healing, here on wounded skin with basic pH, the drug release will be higher than the normal skin with acidic pH.

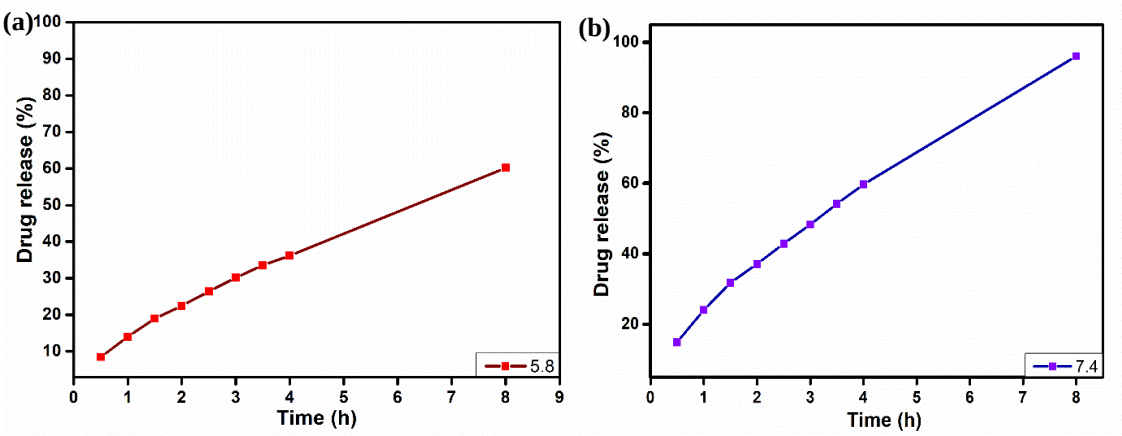

Figure 3.14 Cumulative drug release percentage of the hydrogel at pH of (a) 5.8 and (b) 7.4

3.5 Conclusion

In this chapter, we have successfully developed a facile method for synthesizing biocompatible hydrogels with repeatable adhesive properties. The hydrogel developed in this chapter shows superior adhesive and mechanical strength compared to the hydrogel developed in Chapter 2. In addition, the balance between the covalent and non-covalent interactions within the hydrogel provides reversible stretchability to the hydrogel. This depicts its durability and long-term stability during its application. Moreover, the dynamic covalent and non-covalent interaction provides the hydrogel with stimuli-free self-healing behavior. Furthermore, the swelling behavior of the hydrogel demonstrates its pH sensitivity. Therefore, the pH-responsive *in vitro* drug release behavior shows its possibility as a therapeutic material for wound healing or as a drug reservoir for transdermal use. In summary, the hydrogel synthesized in this chapter shows optimum swelling behavior while maintaining excellent reversible adhesiveness to diverse surfaces with self-healing properties. Hence, the developed hydrogel emerges as a potential biomaterial for various biomedical applications such as drug delivery, wound healing, tissue sealant, etc.

References

[1] Sun, X., He, S., Qin, Z., Li, J. and Yao, F. Fast self-healing zwitterion nanocomposite hydrogel for underwater sensing. *Composites Communications*, 26:100784, 2021.

[2] Cho, E., Lee, J.S. and Webb, K. Formulation and characterization of poloxamine-based hydrogels as tissue sealants. *Acta Biomaterialia*, 8(6):2223-2232, 2012.

[3] Narkar, A.R., Barker, B., Clisch, M., Jiang, J. and Lee, B.P. pH responsive and oxidation resistant wet adhesive based on reversible catechol–boronate complexation. *Chemistry of Materials*, 28(15):5432-5439, 2016.

[4] Zhang, Y., Chen, Q., Dai, Z., Dai, Y., Xia, F. and Zhang, X. Nanocomposite adhesive hydrogels: From design to application. *Journal of Materials Chemistry B*, 9(3):585-593, 2021.

[5] Lu, Y., Huang, X., Luo, Y., Zhu, R., Zheng, M., Yang, J. and Bai, S. Silk fibroin-based tough hydrogels with strong underwater adhesion for fast hemostasis and wound sealing. *Biomacromolecules*, 24(1):319-331, 2022.

[6] Han, D., Farino, C., Yang, C., Scott, T., Browe, D., Choi, W., Freeman, J.W. and Lee, H. Soft robotic manipulation and locomotion with a 3D printed electroactive hydrogel. *ACS Applied Materials & Interfaces*, 10(21):17512-17518, 2018.

[7] Thangavel, P., Ramachandran, B., Chakraborty, S., Kannan, R., Lonchin, S. and Muthuvijayan, V. Accelerated healing of diabetic wounds treated with L-glutamic acid loaded hydrogels through enhanced collagen deposition and angiogenesis: An *in vivo* study. *Scientific Reports*, 7(1):10701, 2017.

[8] Bovone, G., Dudaryeva, O.Y., Marco-Dufort, B. and Tibbitt, M.W. Engineering hydrogel adhesion for biomedical applications *via* chemical design of the junction. *ACS Biomaterials Science & Engineering*, 7(9):4048-4076, 2021.

[9] Romero, I.L., Malta, J.B., Silva, C.B., Mimica, L.M., Soong, K.H. and Hida, R.Y. Antibacterial properties of cyanoacrylate tissue adhesive: Does the polymerization reaction play a role?. Indian Journal Of Ophthalmology, 57(5):341-344, 2009.

[10] Liang, Y., Zhao, X., Hu, T., Chen, B., Yin, Z., Ma, P.X. and Guo, B. Adhesive hemostatic conducting injectable composite hydrogels with sustained drug release and photothermal antibacterial activity to promote full-thickness skin regeneration during wound healing. *Small*, 15(12):1900046, 2019.

[11] Zhao, L., Ren, Z., Liu, X., Ling, Q., Li, Z. and Gu, H. A multifunctional, self-healing, self-adhesive, and conductive sodium alginate/poly (vinyl alcohol)

composite hydrogel as a flexible strain sensor. *ACS Applied Materials & Interfaces*, 13(9):11344-11355, 2021.

[12] Han, G.Y., Park, J.Y., Lee, T.H., Yi, M.B. and Kim, H.J. Highly resilient dual-crosslinked hydrogel adhesives based on a dopamine-modified crosslinker. *ACS Applied Materials & Interfaces*, 14(32):36304-36314, 2022.

[13] Ni, C., Chen, D., Wen, X., Jin, B., He, Y., Xie, T. and Zhao, Q. High speed underwater hydrogel robots with programmable motions powered by light. Nature Communications, 14(1):7672, 2023.

[14] Xia, B. and Chen, G. Research progress of natural tissue-derived hydrogels for tissue repair and reconstruction. *International Journal of Biological Macromolecules*, 214:480-491, 2022.

[15] Pinnataip, R. and Lee, B.P. Oxidation chemistry of catechol utilized in designing stimuli-responsive adhesives and antipathogenic biomaterials. *Acs Omega*, 6(8):5113-5118, 2021.

[16] Wu, L., Li, L., Qu, M., Wang, H. and Bin, Y. Mussel-inspired self-adhesive, antidrying, and antifreezing poly (acrylic acid)/bentonite/polydopamine hybrid glycerol-hydrogel and the sensing application. *ACS Applied Polymer Materials*, 2(8):3094-3106, 2020.

[17] Bennison, L.R., Miller, C.N., Summers, R.J., Minnis, A.M.B., Sussman, G. and McGuiness, W. The pH of wounds during healing and infection: a descriptive literature review. *Wound Practice & Research: Journal of the Australian Wound Management Association*, 25(2):63-69, 2017.

[18] Wang, Y., Adokoh, C.K. and Narain, R. Recent development and biomedical applications of self-healing hydrogels. *Expert Opinion on Drug Delivery*, 15(1):77-91, 2018.

[19] Han, L., Yan, L., Wang, K., Fang, L., Zhang, H., Tang, Y., Ding, Y., Weng, L.T., Xu, J., Weng, J. and Liu, Y. Tough, self-healable and tissue-adhesive hydrogel with tunable multifunctionality. *NPG Asia Materials*, 9(4):e372-e372, 2017.

[20] Xue, B., Gu, J., Li, L., Yu, W., Yin, S., Qin, M., Jiang, Q., Wang, W. and Cao, Y. Hydrogel tapes for fault-tolerant strong wet adhesion. *Nature Communications*, 12(1):7156, 2021.

[21] Balavigneswaran, C.K., Jaiswal, V., Venkatesan, R., Karuppiah, P.S., Sundaram, M.K., Vasudha, T.K., Aadinath, W., Ravikumar, A., Saravanan, H.V. and Muthuvijayan, V. Mussel-inspired adhesive hydrogels based on Laponite-confined dopamine polymerization as a transdermal patch. *Biomacromolecules*, *24*(2):724-738, 2023.

[22] Das, D., Roy, A. and Pal, S. A polysaccharide-based ph-sensitive hybrid hydrogel as a sustained release matrix for antimicrobial drugs. *ACS Applied Polymer Materials*, *5*(5):3348-3358, 2023.

[23] Farasati Far, B., Naimi-Jamal, M.R., Jahanbakhshi, M., Hadizadeh, A., Dehghan, S. and Hadizadeh, S. Enhanced antibacterial activity of porous chitosan-based hydrogels crosslinked with gelatin and metal ions. *Scientific Reports*, *14*(1):7505, 2024.

[24] Xu, Z., Han, S., Gu, Z. and Wu, J. Advances and impact of antioxidant hydrogel in chronic wound healing. *Advanced Healthcare Materials*, *9*(5):1901502, 2020.

[25] Huang, C., Dong, L., Zhao, B., Lu, Y., Huang, S., Yuan, Z., Luo, G., Xu, Y. and Qian, W. Anti-inflammatory hydrogel dressings and skin wound healing. *Clinical and Translational Medicine*, *12*(11):e1094, 2022.

[26] Liebscher, J. Chemistry of polydopamine–scope, variation, and limitation. *European Journal of Organic Chemistry*, *2019*(31-32):4976-4994, 2019.

[27] Hu, X., Ke, Y., Zhang, M., Niu, H., Wu, D. and Zhao, L. Understanding the self-polymerization mechanism of dopamine by molecular simulation and applying dopamine surface modification to improve the interfacial adhesion of polyimide fibers with epoxy resin matrix. *High Performance Polymers*, *33*(6):601-614, 2021.

[28] Wu, L., Li, L., Qu, M., Wang, H. and Bin, Y. Mussel-inspired self-adhesive, antidrying, and antifreezing poly (acrylic acid)/bentonite/polydopamine hybrid glycerol-hydrogel and the sensing application. *ACS Applied Polymer Materials*, *2*(8):3094-3106, 2020.

[29] Wei, Q., Zhang, F., Li, J., Li, B. and Zhao, C. Oxidant-induced dopamine polymerization for multifunctional coatings. *Polymer Chemistry*, *1*(9):1430-1433, 2010.

[30] Salomäki, M., Marttila, L., Kivelä, H., Ouvinen, T. and Lukkari, J. Effects of pH and oxidants on the first steps of polydopamine formation: A thermodynamic approach. *The Journal of Physical Chemistry B*, *122*(24):6314-6327, 2018.

[31] El-Nemr, K.F., Mohamed, H.R., Ali, M.A., Fathy, R.M. and Dhmees, A.S. Polyvinyl alcohol/gelatin irradiated blends filled by lignin as green filler for antimicrobial packaging materials. *International Journal of Environmental Analytical Chemistry*, 100(14):1578-1602, 2020.

[32] Gautam, S., Dinda, A.K. and Mishra, N.C. Fabrication and characterization of PCL/gelatin composite nanofibrous scaffold for tissue engineering applications by electrospinning method. *Materials Science and Engineering: C*, 33(3):1228-1235, 2013.

[33] Bukhari, S.M.H., Khan, S., Rehanullah, M. and Ranjha, N.M. Synthesis and Characterization of Chemically Cross-Linked Acrylic Acid/Gelatin Hydrogels: Effect of pH and Composition on Swelling and Drug Release. *International Journal of Polymer Science*, 2015(1):187961, 2015.

[34] Hina, M., Bashir, S., Kamran, K., Ramesh, S. and Ramesh, K. Synthesis and characterization of self-healable poly (acrylamide) hydrogel electrolytes and their application in fabrication of aqueous supercapacitors. *Polymer*, 210:123020, 2020.

[35] Das, M.P., Suguna, P.R., Prasad, K.A.R.P.U.R.A.M., Vijaylakshmi, J.V. and Renuka, M. Extraction and characterization of gelatin: a functional biopolymer. *International Journal of Pharmacy and Pharmaceutical Sciences*, 9(9):239, 2017.

[36] Pal, K., Banthia, A.K. and Majumdar, D.K. Polyvinyl alcohol—gelatin patches of salicylic acid: preparation, characterization and drug release studies. *Journal Of Biomaterials Applications*, 21(1):75-91, 2006.

[37] Pan, M., Nguyen, K.C.T., Yang, W., Liu, X., Chen, X.Z., Major, P.W., Le, L.H. and Zeng, H. Soft armour-like layer-protected hydrogels for wet tissue adhesion and biological imaging. *Chemical Engineering Journal*, 434:134418, 2022.

[38] Shui, T., Pan, M., Li, A., Fan, H., Wu, J., Liu, Q. and Zeng, H. Poly (vinyl Alcohol)(PVA)-based hydrogel scaffold with isotropic ultratoughness enabled

by dynamic amine–catechol interactions. *Chemistry of Materials*, 34(19):8613-8628, 2022.

[39] Yan, Y., Xu, S., Liu, H., Cui, X., Shao, J., Yao, P., Huang, J., Qiu, X. and Huang, C. A multi-functional reversible hydrogel adhesive. *Colloids and Surfaces A: Physicochemical and Engineering Aspects*, 593:124622, 2020.

[40] Ebrahimi, R. Influence of ultrasonic parameters on degradation of acrylic acid/acrylamide copolymer based superabsorbent hydrogels cross-linked with NMBA. *Iranian Polymer Journal*, 21(1):11-20, 2012.

[41] Kabiri, K., Mirzadeh, H. and Zohuriaan-Mehr, M.J. Undesirable effects of heating on hydrogels. *Journal Of Applied Polymer Science*, 110(6):3420-3430, 2008.

[42] Narkar, A.R., Kelley, J.D., Pinnaratip, R. and Lee, B.P. Effect of ionic functional groups on the oxidation state and interfacial binding property of catechol-based adhesive. *Biomacromolecules*, 19(5):1416-1424, 2017.

[43] Cencer, M., Liu, Y., Winter, A., Murley, M., Meng, H. and Lee, B.P. Effect of pH on the rate of curing and bioadhesive properties of dopamine functionalized poly (ethylene glycol) hydrogels. *Biomacromolecules*, 15(8):2861-2869, 2014.